Noname manuscript No.
(will be inserted by the editor)

Expressions for the joint conditional characteristic function of the Heston stochastic volatility model

Jiaqi Liang · Carolyn E. Phelan · Guido Germano

Received: date / Accepted: date

Abstract The characteristic function of a stochastic process has had an important role in quantitative finance since Heston introduced his famous stochastic volatility model and used it to compute option prices with integrals in the Fourier domain. Option pricing with the Fourier transform was then developped further by Carr and Madan, who used the characteristic function of the variance gamma model, and by others. The earliest pricing methods based on the Fourier transform required only the characteristic function of the distribution of the asset price conditioned on its value at an earlier date. Even the original representation of the Heston model, although conditioned on both the initial price and volatility, gives only the characteristic function of the future value of the log return. However, pricing discrete barrier options and callable options such as American options in Fourier space requires the joint conditional characteristic functions (JCCF) of both the log return and the volatility. Two different expressions of the JCCF for the Heston model have been provided independently by Zhylyevskyy and by Griebsch but, prior to this work, have not been validated against each other or numerically against a Monte Carlo simulation. In this paper we fill this gap in the literature. We derive the two expressions in detail, compare them and correct the "little Heston trap" in Zhylyevskyy's expression. We discuss numerical problems caused by the complex logarithm and implement a general solution to make sure that the corrected expressions remain in the principal branch. Additionally, we validate numerically the two expressions computing the empirical characteristic function from a Monte Carlo simulation.

Keywords Heston model · joint conditional characteristic function · complex logarithm · Monte Carlo · empirical characteristic function

1 Introduction

Stochastic volatility models have become increasingly popular since Heston (1993) introduced his model, overcoming the problem that the Black-Scholes assumption of geometric Brownian motion with constant volatility is not consistent with market behaviour. The introduction of stochastic volatility in the Heston model enables practitioners and academics to fit the smile and skew patterns of the volatility surface by adjusting the model parameters; see for example Cui et al. (2017). After Carr and Madan (1999) introduced the fast Fourier transform method for option pricing and tested it on the variance gamma model, characteristic functions have received an increasing amount of attention, in particular the characteristic

Jiaqi Liang
Department of Computer Science, University College London
66–72 Gower Street, London WC1E 6EA, United Kingdom
E-mail: jiaqi.liang.17@ucl.ac.uk

Carolyn E. Phelan
Department of Computer Science, University College London
66–72 Gower Street, London WC1E 6EA, United Kingdom
E-mail: carolyn.phelan.14@ucl.ac.uk

Guido Germano
Department of Computer Science, University College London
Systemic Risk Centre, London School of Economics and Political Science,
Houghton Street, London WC2A 2AE, United Kingdom
E-mail: g.germano@ucl.ac.uk

functions of stochastic volatility models (Albrecher et al., 2007; Lord and Kahl, 2010). In parallel with these developments, pricing methods using the fast Fourier transform method with stochastic volatility models have been devised for exotic options such as American options (Zhylyevskyy, 2010), compound options (Griebsch, 2013) and discretely monitored barrier options (Cai et al., 2021). For pricing discrete barrier options, many methods make use of the idea that the option price can be expressed as an iterative relationship between the price at successive monitoring dates (Fusai et al., 2006; Feng and Linetsky, 2009; Fusai et al., 2016). In order to exploit this iterative relationship computationally with stochastic volatility, we need to have an expression which captures the distribution of the log return *and* volatility at the end of each time step, conditioned on the values of both these quantities at the start of the time step. It therefore follows that we require the joint conditional probability distribution in order to adapt these techniques to stochastic volatility processes. This is also important for callable contracts such as Bermudan options where the payoff at any intermediate time before maturity is dependent on both the price and variance.

Following the development of the original Heston model, there have been a number of issues that have arisen with numerical implementation and discontinuities. The expressions for the characteristic function of the Heston model contain logarithms of complex variables. When this is implemented numerically, the characteristic function can be discontinuous as the majority of software packages restrict the logarithm to the principle branch. Furthermore Albrecher et al. (2007) showed that the original Heston characteristic function suffers from a numerical discontinuity when reaching a maturity threshold and that the second Heston characteristic function formula used by Bakshi et al. (1997), Duffie et al. (2000) and Gatheral (2011) is continuous under almost all combinations of parameters. The remaining gap was filled by Lord and Kahl (2010) who showed how to avoid discontinuities in the exact simulation algorithm of the Heston model. Cui et al. (2017) also presented a new expression for the characteristic function which is numerically continuous and easily differentiable. Whilst the aforementioned literature has combined to effectively solve the discontinuity problems with the original Heston formulation, such numerical problems with the implementation of the JCCF have not been explored up to now.

In this paper we explore and solve a number of issues with the JCCFs devised by Zhylyevskyy and Griebsch. In Sect. 2 we first compare and validate the expression for the joint conditional characteristic function found by Zhylyevskyy and Griebsch. We demonstrate that the expression from Zhylyeveskky suffers from the "little Heston trap" and show how to solve the problem and give more detail on the derivation of the correct formula. We also show that the original Zhylyevskyy joint conditional characteristic function (JCCF) is numerically discontinuous, whereas both the corrected formula and Griebsch's JCCF are numerically continuous. In addition, we propose an easy tool to solve the discontinuous problem, which works well for all the discontinuities caused by the restriction by the software of the calculation to the principle branch. In order to provide additional verification to the work herein, we also provide a validation of both joint conditional characteristic functions using Monte Carlo simulation.

2 Derivation of the joint conditional characteristic function

In this section, we first briefly revisit the model and derive it's JCCF expression using a similar method to the one in Heston (1993), Duffie et al. (2000), Lord and Kahl (2010). Zhylyevskyy also used this derivation method with the result that the expression fell into the "little Heston trap" (Albrecher et al., 2007) and we provide a correction for this. Following on from this in Sect. 2.2 we show that Zhylyevskyy's formulation, the corrected version and Griebsch's formulation are analytically equivalent. We then discuss the numerical problem caused by complex logarithm of original Zhylyevskyy's expression in Sect. 2.5.

2.1 New derivation removing the "little Heston trap"

Under the risk-neutral pricing measure, the Heston stochastic volatility model is defined by the following system of stochastic differential equations (SDE) for the price of the underlying $S(t) \geq 0$ and its variance $v(t) \geq 0$ for $t \geq 0$,

$$dS(t) = rdt + \sqrt{v(t)}dW_1(t), \tag{1}$$

$$dv(t) = \kappa(\theta - v(t))dt + \sigma\sqrt{v(t)}dW_2(t), \tag{2}$$

$$dW_1(t)dW_2(t) = \rho dt \tag{3}$$

where $r \geq 0$ is the constant risk-free interest rate and $W_i(t),\ i = 1, 2$ are two standard Wiener processes and $\rho \in [-1, 1]$ defines their correlation. The instantaneous variance $v = \{v(t), t \geq 0\}$ is a mean-reverting process and κ (mean-reversion speed), θ (long term mean) and σ (volatility of variance) are non-negative constants. If the initial variance is greater than 0, the variance process is almost surely positive if it satisfies the Feller condition $2\kappa\theta \geq \sigma^2$. Usually a negative value of ρ is taken because, due to the leverage effect, a downward movement of the stock price is usually associated with an upward movement of the volatility.

Furthermore, we define the log return of the underlying price, $x(t) = \log \frac{S(t)}{S(0)}$. According to the definition of an affine process by Duffie et al. (2003), Lord and Kahl (2010) observed that the Heston model is not affine as a function of the price of the underlying S and its variance v, but is affine if written as a function of the log return x and v. Applying Itō's formula, we get the SDE for the log return,

$$dx(t) = \left(r - \frac{v(t)}{2}\right) dt + \sqrt{v(t)} dW_1(t). \tag{4}$$

With the SDE of log return with Eq. (4) and variance Eq. (2), $x(T)$ can be expressed as

$$x(T) = x(t) + r\tau - \frac{1}{2}\int_t^T v(s)ds + \frac{\rho}{\sigma}\left(v(T) - v(t) - \kappa\theta\tau + \kappa\int_t^T v(s)ds\right) + \rho\int_t^T \sqrt{v(s)} dW_2(s), \tag{5}$$

where T is the maturity and $\tau = T - t$ the time to maturity. Then as $x(t)$ is an affine process, the JCCF has the form

$$\phi(\xi_x, T; \xi_v, T|x, t; v, t) = \phi(\xi_x, \xi_v, \tau|x, v) = E\left[\exp(i\xi_x x(T) + i\xi_v v(T))|x(t), v(t)\right] \tag{6}$$

$$= \exp[p(\xi_x, \xi_v, \tau) + q(\xi_x, \xi_v, \tau)v(t) + i\xi_x x(t)], \tag{7}$$

where $p := p(\xi_x, \xi_v, \tau)$ and $q := q(\xi_x, \xi_v, \tau)$ can be obtained in closed form solving a set of ordinary differential equations. The derivation of the JCCF starts with the application of Itō's formula to $\phi(\xi_x, \xi_v, \tau|x, v)$, which yields

$$-\frac{\partial\phi}{\partial\tau}dt + \frac{\partial\phi}{\partial x}dx + \frac{\partial\phi}{\partial v}dv + \frac{1}{2}\left(\frac{\partial^2\phi}{\partial x^2}dx^2 + \frac{\partial^2\phi}{\partial v^2}dv^2\right) + \frac{\partial^2\phi}{\partial x\partial v}dxdv. \tag{8}$$

Substituting dx (4) and dv (2) and combining like terms

$$d\phi = \frac{\partial\phi}{\partial x}\sqrt{v}dW_1 + \frac{\partial\phi}{\partial v}\sigma\sqrt{v}dW_2 + \mathcal{D}\phi, \tag{9}$$

where the differential operator $\mathcal{D}$ is defined as

$$\mathcal{D}\phi = \left[-\frac{\partial\phi}{\partial\tau} + \frac{\partial\phi}{\partial x}\left(r - \frac{v}{2}\right) + \frac{\partial\phi}{\partial v}\kappa(\theta - v) + \left(\frac{\partial^2\phi}{\partial x^2} + \frac{\partial^2\phi}{\partial v^2}\sigma^2\right)\frac{v}{2} + \frac{\partial^2\phi}{\partial x\partial v}\rho\sigma v\right] dt. \tag{10}$$

The Feynman-Kac theorem implies the conditional expectation in Eq. (6) is the unique bounded solution for the partial differential equation (PDE) $\mathcal{D}\phi(\xi_x, \xi_v, \tau|x, v) = 0$, i.e.

$$\frac{\partial\phi}{\partial\tau} = \frac{\partial\phi}{\partial x}\left(r - \frac{v}{2}\right) + \frac{\partial\phi}{\partial v}\kappa(\theta - v) + \left(\frac{\partial^2\phi}{\partial x^2} + \frac{\partial^2\phi}{\partial v^2}\sigma^2\right)\frac{v}{2} + \frac{\partial^2\phi}{\partial x\partial v}\rho\sigma v, \tag{11}$$

where $\tau \in [0, T], x \in \mathbb{R}, v \in \mathbb{R}^+$, and subject to the terminal condition

$$\phi(\xi_x, T; \xi_v, T|x, T; v, T) = \phi(\xi_x, \xi_v, 0|x, v) = \exp(i\xi_x x + i\xi_v v), \tag{12}$$

where we have simplified the notation in the second expression for ϕ Partially differentiating Eq. (7) with respect to τ, x and v we obtain

$$\frac{\partial\phi}{\partial\tau} = \left(\frac{\partial p}{\partial\tau} + \frac{\partial p}{\partial\tau}v(t)\right)\phi, \quad \frac{\partial\phi}{\partial x} = i\xi_x\phi, \quad \frac{\partial\phi}{\partial v} = q\phi, \tag{13}$$

$$\frac{\partial^2\phi}{\partial x^2} = (i\xi_x)^2\phi, \quad \frac{\partial^2\phi}{\partial v^2} = q^2\phi, \quad \frac{\partial^2\phi}{\partial x\partial v} = i\xi_x q\phi. \tag{14}$$

After substituting these back into the PDE $\mathcal{D}\phi(\xi_x, \xi_v, \tau|x, v) = 0$, grouping the terms and and dividing by the common factor ϕ, we get

$$-\frac{\partial p}{\partial\tau} + i\xi_x r + \kappa\theta q + v(t)\left[-\frac{\partial q}{\partial\tau} - \frac{1}{2}(\xi_x^2 + i\xi_x) + (i\xi_x\rho\sigma - \kappa)q + \frac{1}{2}\sigma^2 q^2\right] = 0, \tag{15}$$

subject to the initial conditions $q(\xi_x, \xi_v, 0) = i\xi_v$ and $p(\xi_x, \xi_v, 0) = 0$.

As the Eq. (15) must be true for all $\tau \in [0, T]$, $x \in \mathbb{R}$ and $v \in \mathbb{R}^+$, both of the coefficient of v and the constant term must consequently be equal to 0. So we must have the following system of differential equations

$$\frac{dq}{d\tau} + Cq^2 + Dq + E = 0 \tag{16}$$

$$\frac{dp}{d\tau} - i\xi_x r - \kappa\theta q = 0, \tag{17}$$

where $C = -\frac{1}{2}\sigma^2$, $D = -i\xi_x\rho\sigma + \kappa$ and $E = \frac{1}{2}(\xi_x^2 + i\xi_x)$.

Eq. (16) is a Riccati equation which can be solved by defining $y := q - q_1$ and making the change of variable $q = y + q_1$, where q_1 is a known solution of Eq. (16); then the Riccati equation reduces to the Bernoulli equation

$$\frac{dy}{d\tau} = -(2Cp_1 + D)y - Cy^2. \tag{18}$$

Then change the variable again $w := \frac{1}{y}$ and get

$$\frac{dw}{d\tau} = -Zw + C, \tag{19}$$

where $Z = -(2Cp_1 + D)$. Multiplying both sides of Eq. (19) by $e^{Z\tau}$ and using the product rule, the result is

$$\frac{d(we^{Z\tau})}{d\tau} = Ce^{Z\tau}. \tag{20}$$

Integrating both sides with respect to τ, we get the general solution

$$w = \frac{C}{Z} + C_0 e^{-Z\tau}, \tag{21}$$

where $C_0 = w(0) - \frac{C}{Z} = \frac{1}{i\xi_v - q_1} - \frac{C}{Z}$. Changing back the variable q, we get

$$q = \frac{1 + \frac{C}{Z} + \left(\frac{1}{i\xi_v - q_1} - \frac{C}{Z}\right)e^{-Z\tau}}{\frac{C}{Z} + \left(\frac{1}{i\xi_v - q_1} - \frac{C}{Z}\right)e^{-Z\tau}}. \tag{22}$$

q_1 can be found by solving

$$Cq_1^2 + Dq_1 + E = 0. \tag{23}$$

Then there are two solutions,

$$q_{1,\pm} = \frac{-D \pm \sqrt{D^2 - 4CE}}{2C}. \tag{24}$$

Both solutions are analytically equivalent, but the positive square root solution yields numerical problems which the negative one avoids (Albrecher et al., 2007; Cui et al., 2017). This is why the characteristic function cannot be defined when $(\xi_x, \xi_v, \tau \neq 0) = (0, 0, \tau)$ in Zhylyevskyy's paper. We will discuss the problem in detail in Sect. 2.5.

After manipulations we get

$$q = \frac{1}{\sigma^2}\left[\kappa - \rho\sigma i\xi_x + \sqrt{A}\frac{Be^{-\tau\sqrt{A}} - 1}{Be^{-\tau\sqrt{A}} + 1}\right], \tag{25}$$

where

$$A = D^2 - 4CE = (\kappa - \sigma\rho i\xi_x)^2 + \sigma^2(i\xi_x + \xi_x^2) \tag{26}$$

$$B = -\frac{\sigma\rho i\xi_x - \kappa + \sqrt{A} + \sigma^2 i\xi_v}{\sigma\rho i\xi_x - \kappa - \sqrt{A} + \sigma^2 i\xi_v}. \tag{27}$$

We substitute Eq. (25) into Eq. (17) and similarly, with a change of variable and an integration, we obtain the solution

$$p = r\tau i\xi_x + \frac{\kappa\theta}{\sigma^2}\left[(\kappa - \sigma\rho i\xi_x)\tau - \tau\sqrt{A} + 2\log\frac{B + 1}{Be^{-\tau\sqrt{A}} + 1}\right] + p_0, \tag{28}$$

where $p_0 = p(\xi_x, \xi_v, 0) = 0$.

2.2 Comparison

The first closed form of the conditional characteristic function of the Heston model $\phi_{\mathrm{H}}(\xi_x, T|x, t; v, t)$ was found by Heston (1993) himself applying the Feynman-Kac representation theorem. More convenient and numerical stable formulations were proposed later (Bakshi et al., 1997; Duffie et al., 2000; Gatheral, 2011; Cui et al., 2017). However, to price discretely monitored path-dependent options we need the JCCF. Two different expressions of the JCCF for the Heston model were found by Zhylyevskyy (2010) and by Griebsch (2013). The formulation we derived in Sect. 2.1 is equivalent to both expressions and also corrects the numerical problem of Zhylyevskky's expression. We will discuss in detail in this subsection.

2.3 Zhylyevskyy formulation

Zhylyevskyy ygave a JCCF expression which has the same form as ϕ in Eq. (7):

$$\phi_{\mathrm{Z}}(\xi_x, \xi_v, \tau|x, v) = \exp[p_{\mathrm{Z}}(\xi_x, \xi_v, \tau) + q_{\mathrm{Z}}(\xi_x, \xi_v, \tau)v(t) + i\xi_x x(t)], \tag{29}$$

such that

$$p_{\mathrm{Z}} = r\tau i\xi_x + \frac{\kappa\theta}{\sigma^2}\left[(\kappa - \sigma\rho i\xi_x)\tau + \tau\sqrt{A} + 2\log\frac{B_{\mathrm{Z}} + 1}{B_{\mathrm{Z}}e^{\tau\sqrt{A}} + 1}\right], \tag{30}$$

$$q_{\mathrm{Z}} = \frac{1}{\sigma^2}\left[\kappa - \rho\sigma i\xi_x - \sqrt{A}\frac{B_{\mathrm{Z}}e^{\tau\sqrt{A}} - 1}{B_{\mathrm{Z}}e^{\tau\sqrt{A}} + 1}\right], \tag{31}$$

where

$$B_{\mathrm{Z}} = -\frac{\sigma\rho i\xi_x - \kappa - \sqrt{A} + \sigma^2 i\xi_v}{\sigma\rho i\xi_x - \kappa + \sqrt{A} + \sigma^2 i\xi_v} = \frac{1}{B}. \tag{32}$$

We can notice that p_{Z} and p from Eq. (28) are similar, the only differences being the sign in front of $\sqrt{A}$ and the whether B_{Z} or B is used. A similar observation exists for q_{Z} and q. That is due to the fact that the square root of A has two possible solutions, $\sqrt{A}$ and $-\sqrt{A}$. Zhylyevskyy chose to use the principle square root $\sqrt{A}$ whereas in our derivation we used $-\sqrt{A}$. In reality, most mathematical software returns the principal square root, which may introduce discontinuities and other problems. One such problem is that $\phi_{\mathrm{Z}}(0, 0)$ in Eq. (29) is not defined, since

$$\lim_{(\xi_x,\xi_v)\to(0,0)} B_{\mathrm{Z}}(\xi_x, \xi_v) = -\frac{-\kappa - \kappa}{-\kappa + \kappa} = \frac{2\kappa}{0} = \infty. \tag{33}$$

However the problem can be avoided by using $-\sqrt{A}$, as then

$$\lim_{(\xi_x,\xi_v)\to(0,0)} B(\xi_x, \xi_v) = -\frac{-\kappa + \kappa}{-\kappa - \kappa} = 0. \tag{34}$$

With regards the selection of the negative root, although $\phi_{\mathrm{Z}}(0, 0)$ being undefined can be corrected by setting $q_{\mathrm{Z}} = p_{\mathrm{Z}} = 0$ when when $(\xi_x = 0, \xi_v = 0)$, as proved by Zhylyevskyy (2010), the use of $\sqrt{A}$ causes another problem which is the discontinuity of the logarithm of a complex value and this will be discussed in Sect. 2.5. Despite the above issues, the two JCCF formulations, ϕ and ϕ_{Z} are equivalent since we can observe

$$-\tau\sqrt{A} + 2\log\frac{B + 1}{Be^{-\tau\sqrt{A}} + 1} = \tau\sqrt{A} + 2\log\frac{e^{-\tau\sqrt{A}}(1/B + 1)}{e^{-\tau\sqrt{A}}/B + 1} = \tau\sqrt{A} + 2\log\frac{B_{\mathrm{Z}} + 1}{B_{\mathrm{Z}}e^{\tau\sqrt{A}} + 1}, \tag{35}$$

and

$$\sqrt{A}\frac{Be^{-\tau\sqrt{A}} - 1}{Be^{-\tau\sqrt{A}} + 1} = \sqrt{A}\frac{\left(e^{-\tau\sqrt{A}}/B_{\mathrm{Z}} - 1\right)B_{\mathrm{Z}}e^{\tau\sqrt{A}}}{\left(e^{-\tau\sqrt{A}}/B_{\mathrm{Z}} + 1\right)B_{\mathrm{Z}}e^{\tau\sqrt{A}}} = -\sqrt{A}\frac{B_{\mathrm{Z}}e^{\tau\sqrt{A}} - 1}{B_{\mathrm{Z}}e^{\tau\sqrt{A}} + 1} \tag{36}$$

2.4 Griebsch formulation

Griebsch used a different approach than Zhylyevskyy to obtain the JCCF. Instead of setting up a PDE for ϕ and solving it, she wrote the conditional expectation, Eq. (6), using the expression of x given in Eq. (5):

$$\phi_{\mathrm{G}}(\xi_x,\xi_v,\tau|x,v)=\exp(i\xi_x(x(t)+r\tau-\frac{\rho}{\sigma}v(t)-\frac{\rho}{\sigma}\kappa\theta\tau))E\left[\exp(-b\int_t^T v(u)du+av(T))|x(t),v(t)\right], \quad (37)$$

where

$$a=i\xi_v+i\xi_x\frac{\rho}{\sigma}, \quad (38)$$

$$b=-\frac{\kappa\rho}{\sigma}i\xi_x+\frac{1}{2}i\xi_x+\frac{1}{2}\xi_x^2(1-\rho^2). \quad (39)$$

Griebsch (2013) showed that by applying the Feynman-Kac formulation, the expectation

$$E\left[\exp(-b\int_t^T v(u)du+av(T))|x(t),v(t)\right] \quad (40)$$

can be solved and thus the solution to Eq. (37) can be obtained. Readers who are interested can find the detailed derivation in the Appendix of Griebsch (2013). The final JCCF expression that she derived ϕ_{G} is

$$\phi_{\mathrm{G}}(\xi_x,\xi_v,\tau|x,v)=\exp(i\xi_x(x(t)+r\tau-\frac{\rho}{\sigma}v(t)-\frac{\rho}{\sigma}\kappa\theta\tau))\exp\left(p_{\mathrm{G}}(a,b,\tau)+q_{\mathrm{G}}(a,b,\tau)v(t)\right), \quad (41)$$

with

$$p_{\mathrm{G}}(a,b,\tau)=\frac{\kappa\theta}{\sigma^2}\left(\kappa\tau-d\tau+2\log\frac{2d}{\gamma}\right), \quad (42)$$

$$q_{\mathrm{G}}(a,b,\tau)=\frac{-(1-e^{-d\tau})(2b+\kappa a)+da(1+e^{-d\tau})}{\gamma}, \quad (43)$$

where

$$d=\sqrt{\kappa^2+2\sigma^2 b} \quad (44)$$

$$\gamma=2de^{-d\tau}+(\kappa+d-\sigma^2 a)(1-e^{-d\tau}). \quad (45)$$

Griebsch's expression of the JCCF looks different from Zhylyevskyy's, but with a number of manipulations we found they are equivalent and exactly same as the corrected Zhylyevskyy expression which we provided. One important relationship we can observe through careful manipulations and compare ϕ and ϕ_{G} is $d^2=A$. In addition, same as our result, Griebsch also chose to use $-d$ i.e. $-\sqrt{A}$, therefore also avoiding numerical issues. We then can notice the sum of B's numerator and denominator is equal to $2\sqrt{A}$ and we find

$$\log\frac{2d}{\gamma}=\log\left(\frac{2\sqrt{A}}{2\sqrt{A}e^{-\tau\sqrt{A}}+(\kappa+\sqrt{A}-\sigma^2 i\xi_v-\sigma\rho i\xi_x)(1-e^{-\tau\sqrt{A}})}\right)=\log\frac{B+1}{Be^{-\tau\sqrt{A}}+1}, \quad (46)$$

which involve the complex logarithm and will be analysed in Sect. 2.5 then we can prove $\phi_{\mathrm{Z}}=\phi=\phi_{\mathrm{G}}$ accordingly.

Despite the undefined $\phi_{\mathrm{Z}}(0,0,\tau)$, the three JCCF formulations are equivalent. However with the choice of using the principle square root $\sqrt{A}$, ϕ_{Z} will suffer from the numerical problem and we will discuss the detail in the next section.

Table 1: Heston model and market parameters.

Model parameters		Market parameters	
κ	4	$x(0)$	100
θ	0.035	r	0.05
σ	0.15		
ρ	-0.6		
$v(0)$	0.04		

2.5 Complex discontinuity

The previous three expressions of closed form Heston JCCF include the logarithm of a complex variable. Depending on which branch is taken in the calculation, this may cause discontinuities in the complex plane. Consider a complex variable $z = \alpha + \beta i$ and $z = \omega e^{i\delta}$, where r and θ are radius and argument of z. Then by taking the logarithm of z, we get

$$\log(z) = \log(|\omega|) + i\delta. \tag{47}$$

The problem will occur if δ is not in the range $(-\pi, \pi]$, which is called the principle branch; Note that the imaginary part of $\log(z)$ is δ which is the argument of z. As most of programming languages will return δ within the principle branch; discontinuities will therefore occur when δ falls below $-\pi$ or rises above π and the results returned will be $\delta + 2\pi$ or $\delta - 2\pi$ respectively. This is shown in Fig. 1 which plots the imaginary part of $\log(z)$ for $\delta \in [0, 5\pi]$. The original expression is shown with the red dotted line and the results calculated using Matlab are shown with the blue solid line and we can notice the discontinuities which occur when $\mathrm{Im}(\log(z)) = k2\pi$

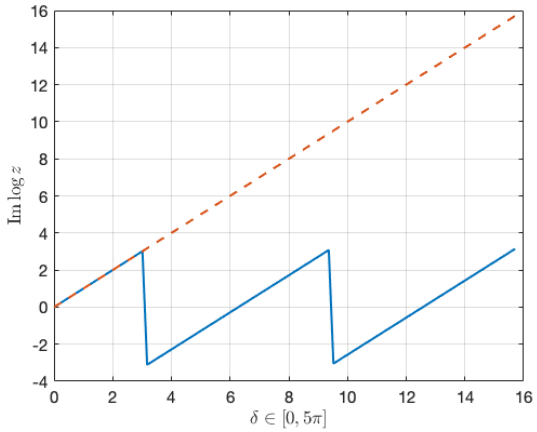

Fig. 1: Example of discontinuity of the imaginary part of $\log(z)$ calculated by Matlab.

In this section, we will first test the continuity of the complex plane for the JCCFs in Zhylyevskyy's and Griebsch's paper. Then we will propose a solution to solve the discontinuity problem not only for Heston JCCF but also for all the discontinuity caused by the restriction of the imaginary part by the programming language.

In Sect. 2.2 we proved the three JCCF expressions are equivalent. We can then find the following equations

$$f_1 = \tau\sqrt{A} + 2\log\frac{B_Z + 1}{B_Z e^{\tau\sqrt{A}} + 1}, \tag{48}$$

$$f_2 = -\tau\sqrt{A} + 2\log\frac{B + 1}{Be^{-\tau\sqrt{A}} + 1}, \tag{49}$$

$$f_3 = -d\tau + 2\log\frac{2d}{\gamma}, \tag{50}$$

from Zhylyevskyy's, our corrected Zhylyevskyy's and Griebsch's JCCF formulations which are analytically equal, i.e. $f_1 = f_2 = f_3$. we can expect f_1, f_2 and f_3 to return the same result for all appropriate (ξ_x, ξ_v). However, in Fig. 2, we can notice that if we fix ξ_v and plot $\mathrm{Im}(\log(f_i)), i = 1, 2, 3$ with $\xi_x \in [0, 10]$, the blue line f_1 from Zhylyevskyy's expression is different from other two. The zigzag pattern of f_1 caused by the restriction of logarithm to its principal branch, in common with most programming languages. In contrast, the corrected Zhylyevskyy's and Griebsch's expressions, i.e. f_2 and f_3, do not suffer from the branch switching problem with increasing ξ_x. We can observe why this only effects f_1 by considering the

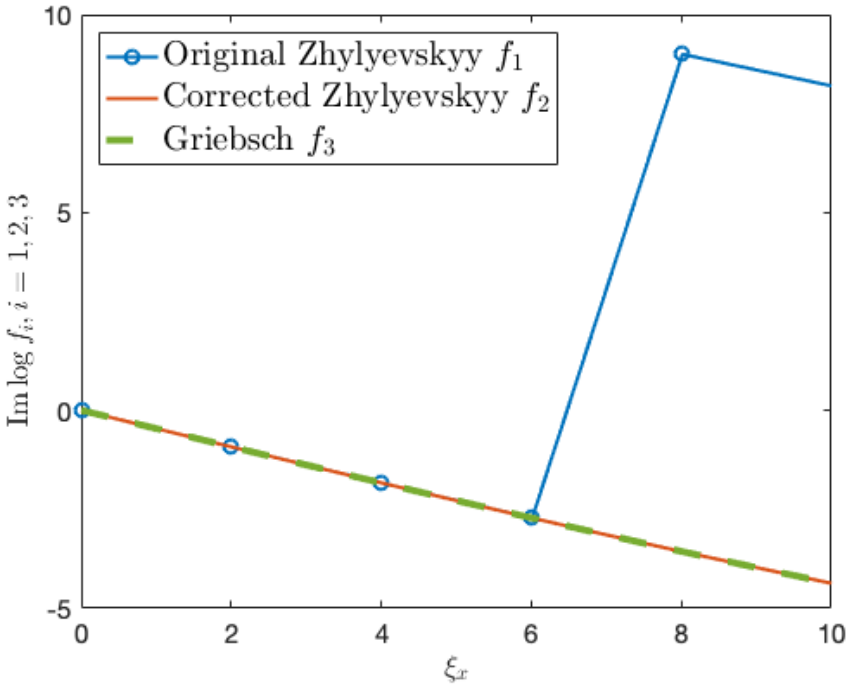

Fig. 2: The imaginary part of three equivalent expressions $\mathrm{Im}(\log(f_i)), i = 1, 2, 3$. The curves are generated using the parameters in Table 1 with $\xi_x \in [0, 10]$, $\tau = 5$ and fixed $\xi_v = 1.0127$.

following function which is the second expression in Eq. 48:

$$F_1(\xi_x, \xi_v) = \frac{B_\mathrm{Z} + 1}{B_\mathrm{Z} e^{\tau\sqrt{A}} + 1}. \tag{51}$$

The similar function in the corrected Zhylyevskyy JCCF is formulated as

$$F_2(\xi_x, \xi_v) = \frac{B + 1}{B e^{-\tau\sqrt{A}} + 1}. \tag{52}$$

To illustrate the problem of branch cut with these two functions, we plot the trajectory $\lambda(\xi_x, \xi_v)$, as formulated by Albrecher et al. (2007); Kahl and Jäckel (2005), of F_1 and F_2 on the complex plane. This is calculated as

$$\lambda_i(\xi_x, \xi_v) = F_i(\xi_x, \xi_v) \frac{\log\log|F_i(\xi_x, \xi_v)|}{|F_i(\xi_x, \xi_v)|}, \quad i = 1, 2. \tag{53}$$

where one of the double logarithms is due to the fact that one is applied F_i in the JCCF and the other is to compensate for the rapidly growing radius and outward movement of the spiralling trajectory of F_1.

In Fig. 3a, we can see clearly the spiral shape of λ_1 and that its trajectory crosses the negative real axis in the complex plane. In contrast, we can see from Fig. 3b that the trajectory of λ_2 does not cross the negative real axis. The repeated crossing of the negative real axis caused the discontinuity as the principle value of δ jumps between the extremes of the range $(-\pi, \pi]$. The outward movement of the spiralling trajectory of F_1 is due to the fact that $e^{\tau\sqrt{A}}$ is a spiral with exponentially growing radius when $\mathrm{Im}(\sqrt{A}) \neq 0$. Here we can rewrite the logarithm of F_1 as

$$\log F_1 = -(-\log F_1) = -\log \frac{B_\mathrm{Z} e^{\tau\sqrt{A}} + 1}{B_\mathrm{Z} + 1}, \tag{54}$$

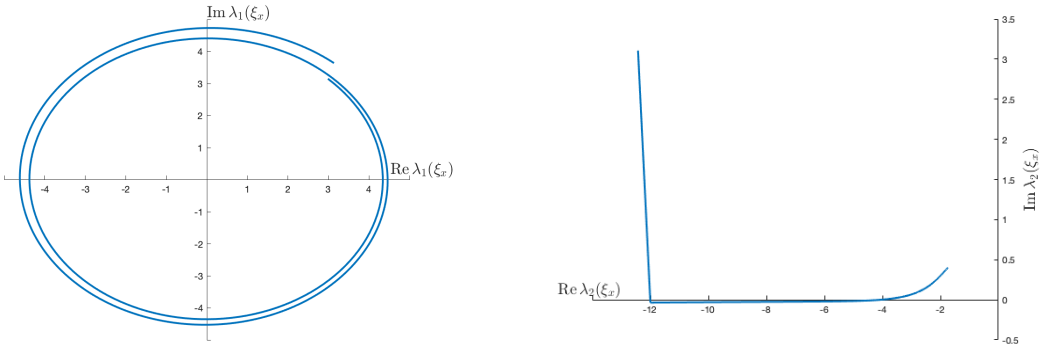

(a) Trajectory of λ_1. (b) Trajectory of λ_2.

Fig. 3: Trajectories of $\lambda_i(\xi_x, \xi_v), i = 1, 2$, where $\xi_x \in [0, 50], \xi_v = 1.0127$ in the complex plane with $\tau = 5$. The plots are generated using the parameters in Table 1.

and if τ is large enough, F_1 is dominated by $e^{\tau\sqrt{A}}\frac{B_Z}{B_Z+1}$ the value of the imaginary part of $\log F_1$ will be greater than π and the discontinuity will occur when switching the branch.

In order to avoid the branching cut problem when implementing the solution numerically, one solution is to use the JCCF formulations ϕ and ϕ_g which do not involve branch switching in the complex logarithm. Another way is to use the `unwrap(P)` where P is the vector or matrix of angles in Matlab. This function monitors the jump between consecutive angles of `P`. If the jump is greater than or equal to π, `unwrap` shifts the angles by adding multiples of $\pm 2\pi$ until the jump is less than π. There is an alternative algorithm for solving this discontinuity problem introduced by Kahl and Jäckel (2005) and verified by Lord and Kahl (2006). Instead of monitoring every jump between consecutive angles of `P` they count the number of how many circles of `P` rotated in the complex plane and add the number of rotation times 2π to the restricted argument to make it continuous. In our case we take P is equal to $\text{Im}(\log(F_1))$, then f_1 with the application of unwrap can be found by following Matlab code:

```
ImagPart = unwrap(imag(log(F1)));
RealPart = real(log(F1));
f4 = tau*sqrt(A) + 2*complex(RealPart,ImagPart)
```

The resulting calculation of f_4 does not suffer from the problem of discontinuities in the complex plane this is illustrated in Fig. 4.

2.6 Using the `unwrap(P)` function with the Broadie and Kaya (2006) method

The `unwrap(P)` function can also be applied to other cases which involve branch switching on the complex plane. One of the application is for the exact simulation algorithm of the Heston model which published by Broadie and Kaya (2006). This method generates exact samples of $S(T)$ from its distribution conditioned on the value of variance which has been generated by the variance process. The main advantage of the exact simulation over the conventional Euler discretisation is it has faster convergence rate which leads to lower computational time for achieving high accuracy. This exact simulation method can also be applied to price exotic path dependent options as the required transition probability density can be found by taking the inverse Fourier transform of the JCCF found by the exact simulation The full algorithm is beyond the purpose of the paper, however one of the important and relevant steps is to simulate $\int_t^T v(u)du$ given $v(t)$ and $v(T)$. As the distribution of $\int_t^T v(u)du$ is unknown in closed form, Broadie and Kaya found

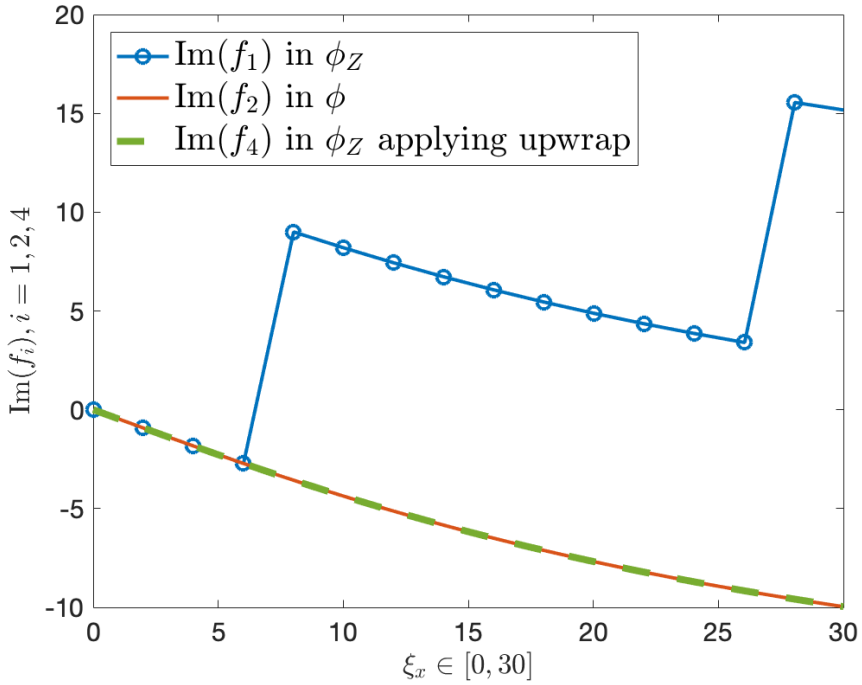

Fig. 4: The imaginary part of f_1, f_2 and f_4 where f_4 is f_1 with application of `unwrap` function in Matlab. The curves are generated using the parameters in Table 1 with $\xi_x \in [0, 10]$, $\tau = 5$ and fixed $\xi_v = 1.0127$.

the probability function by taking the inverse Fourier transform of the characteristic function

$$\begin{aligned}\Phi(\xi) &= E\left[\exp\left(i\xi\int_t^T v(u)du\right)|v(t), v(T)\right] \\ &= \frac{\eta(\xi)e^{(-1/2)(\eta(\xi)-\kappa)\tau}(1-e^{-\kappa\tau})}{\kappa(1-e^{-\eta(\xi)\tau})} \\ &\quad\times \exp\left\{\frac{v(t)+v(T)}{\sigma^2}\left[\frac{\kappa(1+e^{-\kappa\tau})}{1-e^{-\kappa\tau}} - \frac{\eta(\xi)(1+e^{-\eta(\xi)\tau})}{1-e^{-\eta(\xi)\tau}}\right]\right\} \\ &\quad\times \frac{I_\nu\left(\sqrt{v(t)v(T)}\frac{4\eta(\xi)e^{-0.5\eta(\xi)\tau}}{\sigma^2(1-e^{-\eta(\xi)\tau})}\right)}{I_\nu\left(\sqrt{v(t)v(T)}\frac{4\kappa e^{-0.5\kappa\tau}}{\sigma^2(1-e^{-\kappa\tau})}\right)},\end{aligned} \tag{55}$$

where $\eta(\xi) = \sqrt{\kappa^2 - 2\sigma^2 i\xi}$, $\nu = 2\kappa\theta/\sigma^2 - 1$ is the number of degrees of freedom and $I_\nu(\cdot)$ is the modified Bessel function of the first kind. Therefore

$$I_\nu(z) = \left(\frac{1}{2}z\right)^\nu \sum_{j=0}^{\infty} \frac{(\frac{1}{4}\nu^2)^j}{j!\Gamma(\nu+j+1)}, \tag{56}$$

where z is a complex number and $\Gamma(\cdot)$ is the gamma function . Broadie and Kaya found that $I_\nu(z)$ has a branch switching problem which causes the characteristic function (55) to be discontinuous. That is because, in order to evaluate $I_\nu\left(\sqrt{v(t)v(T)}\frac{4\eta(\xi)e^{-0.5\eta(\xi)\tau}}{\sigma^2(1-e^{-\eta(\xi)\tau})}\right)$ in Eq. (55) we need to calculate z^ν in Eq. (56) as $\exp(\nu\log(z))$, where the complex logarithm causes the discontinuity. In addition, in order to avoid the problem caused by the denominator $I_\nu\left(\sqrt{v(t)v(T)}\frac{4\kappa e^{-0.5\kappa\tau}}{\sigma^2(1-e^{-\kappa\tau})}\right)$ tends to 0, we compute the fraction with two modified Bessel functions, i.e.

$$\frac{I_\nu\left(\sqrt{v(t)v(T)}\frac{4\eta(\xi)e^{-0.5\eta(\xi)\tau}}{\sigma^2(1-e^{-\eta(\xi)\tau})}\right)}{I_\nu\left(\sqrt{v(t)v(T)}\frac{4\kappa e^{-0.5\kappa\tau}}{\sigma^2(1-e^{-\kappa\tau})}\right)} \tag{57}$$

as

$$\exp\left(\log\left[\sqrt{v(t)v(T)}\frac{4\eta(\xi)e^{-0.5\eta(\xi)\tau}}{\sigma^2(1-e^{-\eta(\xi)\tau})}\right]-\log\left[\sqrt{v(t)v(T)}\frac{4\kappa e^{-0.5\kappa\tau}}{\sigma^2(1-e^{-\kappa\tau})}\right]\right). \tag{58}$$

Lord and Kahl (2010) provide a solution that is to find an expression which equivalent to $\frac{\eta(\xi)e^{-0.5\eta(\xi)\tau}}{1-e^{-\eta(\xi)\tau}}$ but continuous on the complex plane. One practical difficulty of this method is that users need to write efficient code for the modified Bessel function I_ν instead of directly calling the function in the library. However this problem can be solved by using the `unwrap` function. In this case we are not required to find the equivalent expression and instead only need to apply the `unwrap` function to the complex logarithm of the numerator of Eq. (57) as the denominator is a real number. By defining

$$h(\xi)=\log\left[\sqrt{v(t)v(T)}\frac{4\eta(\xi)e^{-0.5\eta(\xi)\tau}}{\sigma^2(1-e^{-\eta(\xi)\tau})}\right], \tag{59}$$

we can compare the imaginary part of $h(\xi)$ with and without applying `unwrap` in Fig. 5. We can observe

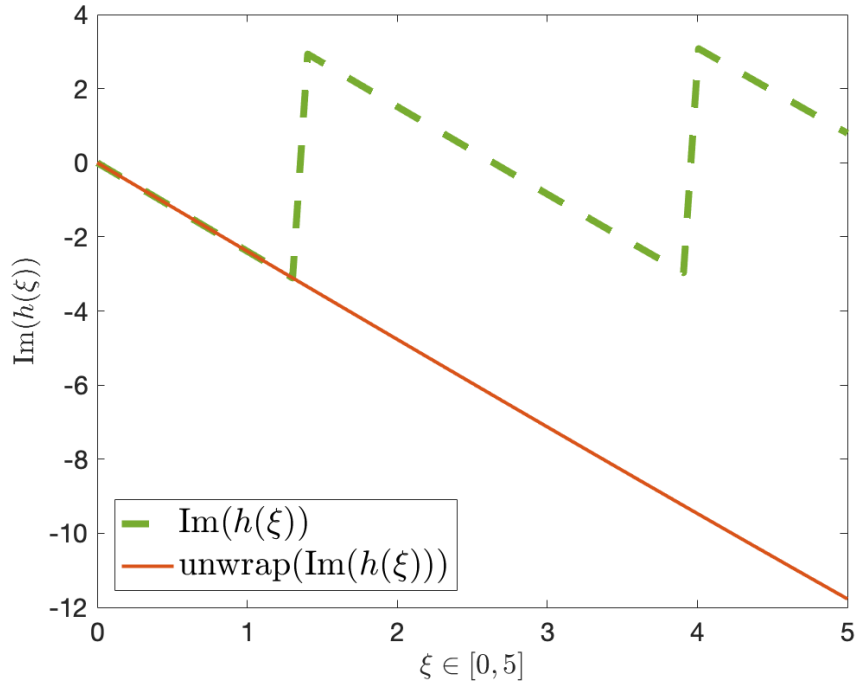

Fig. 5: The imaginary part of $h(\xi)$ with and without the application of `unwrap` function in Matlab. The curves are generated using the parameters in Table 1 with $\xi_x \in [0,5]$, $v(t)=0.04$, $v(T)=0.045$ and $\tau=5$.

the discontinuity in the complex plane can be easily solved by calling the `unwrap` function.

3 Numerical results

In Sect. 2.2 we proved that the three JCCF expressions ϕ, ϕ_{Z} and ϕ_{G} are analytically equivalent, although ϕ_{Z} suffers from the numerical discontinuity problem which we discussed in Sect. 2.5. In this section we show the results of the numerical evaluations that were carried out. We validate the three formulations ϕ, ϕ_{Z} and ϕ_{G} by the empirical joint characteristic function (EJCCF) and the numerical JCCF approximated from the joint histogram generated by a Monte Carlo simulation of 10^6 paths with maturity $T=1$ discretised to $\Delta T=0.01$ steps. We compute the root mean squared error (RMSE) and the maximum absolute error (MAE) to assess the differences numerically. The model and market parameters we used are shown in Table. 1.

3.1 Validation

We used two methods to validate the three JCCF expressions. As we mention above, one method is to perform a Monte-Carlo simulation based on the original SDEs to obtain simulated values for $(x_j(T), v_j(T)), j \in M$, we can then obtain the 3D histogram plotted with log return and variance axes. The histogram is the approximation of the joint conditional probability distribution function (JCPDF) of Heston model. We can then calculate the JCCF by applying 2D Fourier transform to the JCPDF. Alternatively by simulating log return and variance we can directly calculate the EJCCF using

$$\phi_{\mathrm{e}}(\xi_x, \xi_v) = \frac{1}{M}\left(\sum_{j=1}^{M} \exp(i\xi_x x_j) \times \overline{M} \sum_{j=1}^{M} \exp(i\xi_v v_j)\right), \tag{60}$$

where x_j and v_j are the values at maturity and M is the number of Monte Carlo paths. The resulting benchmark figures can be found in Fig. 6a and Fig. 6b.

The JCCF plots from the two different methods are the same. By representing the three JCCF formulations ϕ, ϕ_{Z} and ϕ_{G} in Figs. 6e, 6d, 6c respectively, we observe that ϕ and ϕ_{G} produce the plots matching the benchmarks. It is unsurprising that ϕ and ϕ_{G} have the same plot because we proved the two expressions are exactly identical in Sect. 2.2. In addition, by observing that Figs. 6a, 6b, 6c, 6e are identical we can validate the correctness of both ϕ and ϕ_{G}. In contrast, when we examine Fig. 6d, one can notice that although everything else matches, the function is undefined at the point $(\xi_x = 0, \xi_v = 0)$ due to the choice of using the principal square root, as discussed in Sect. 2.2.

We further validate the expressions ϕ and ϕ_{G} by applying a 2D inverse Fourier transform to obtain the JCPDFs which are compared with the 2D histogram. The results shown in Fig. 7. Again we verify that both expressions ϕ and ϕ_{G} are correct as they match the histogram.

In addition, we verified the JCCF analytical expressions ϕ and ϕ_{G} by examining the relationship between the JCCF expression and the well-known conditional characteristic function (CCF) for Heston model. We noticed that although there are various ways of expressing the Heston CCF ϕ_{H}, these are based are two main formulations. The first of these can be found from the in the original paper of Heston. However as reported by Lord and Kahl (2010) and Albrecher et al. (2007), the original Heston CCF also suffers from the problem of numerical discontinuities in the complex plane, in the same way as we observed in Zhylyevskyy's expression for the JCCF. Therefore here we opt use the second conditional characteristic function from Bakshi et al. (1997) for the validation. The idea is to compute the log return marginal conditional probability functions from different JCCF expressions ϕ and ϕ_{G} and compare these with the CCF ϕ_{H}. By applying an inverse Fourier transform to ϕ_{H} it is also straightforward to obtain the marginal conditional probability functions for log return. In contrast, when we begin with the JCCF, ϕ or ϕ_{G}, we need an extra step which is taking the 2D inverse Fourier transform to ϕ or ϕ_{G} to obtain the JCPDF. We can then integrate the JCPDF with respect to variance to get the log return marginal conditional probability functions. Furthermore, the marginal probability functions calculated from the analytical expressions can also be assessed by comparing them with the numerical marginal probability functions computed from numerically integrating the 2D histogram. Fig. 8 provides a summary of the resulting marginal probability functions derived from ϕ_{H}, ϕ, ϕ_{G} and the approximation from the histogram and it can be seen that the plots match each other. It is not unexpected that the probability functions computed from ϕ, ϕ_{G} and histogram are same as they have same JCPDF in Fig. 7, but by confirming that the Heston CCF gives the same result, we can verify there is a relationship between the above analytical JCCF expressions (i.e. ϕ and ϕ_{G}) and the CCF, thus providing additional validation of the correctness of the JCCF expressions.

3.2 Error analysis

In Sect. 3.1 we present the plots for the comparison of the for Griebsch and corrected Zhylyevskyy expressions and the Monte Carlo approximation. These were carried out for a single set of process parameters defined in Table 1 and there is no observable difference among the JCCF and JCPDF figures. Therefore, for more comprehensive validation result we expand our tests to a number of different sets of model parameters which are randomly chosen from the range given in Table 2. For each selected parameter set, we calculate the mean-squared error (RMSE) and the maximum absolute deviation (MAE). We summarised the final result in average in Table 3 and Table 4.

The RMSE measures the average squared difference between the testing values and the benchmark values. In Table 3, the testing values are the JCCFs and JCPDFs obtained from analytical expressions ϕ_{Z},

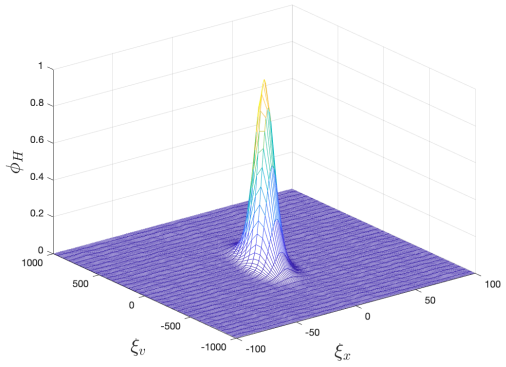

(a) Histogram with 2D Fourier transform

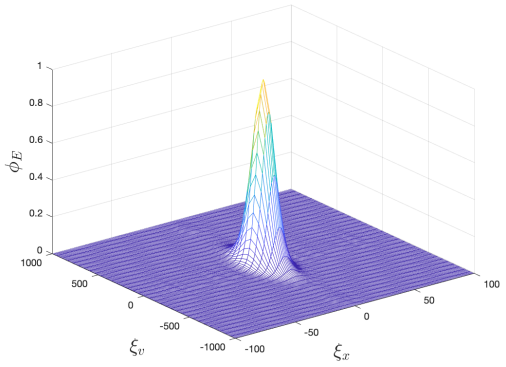

(b) EJCCF

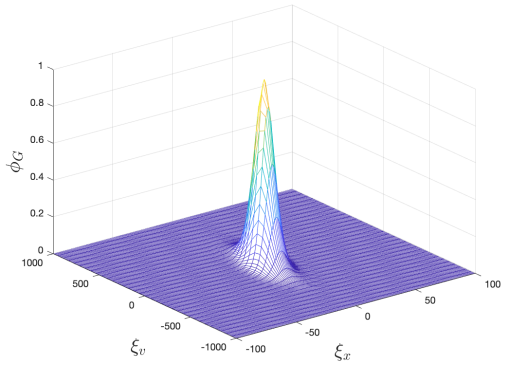

(c) Griebsch

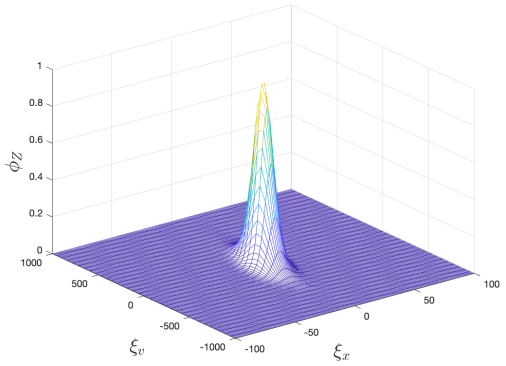

(d) Zhylyevskyy

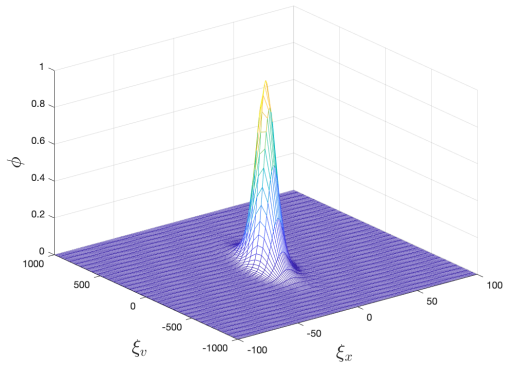

(e) Corrected Zhylyevskyy

Fig. 6: Joint conditional characteristic function (JCCF) at maturity T from a Monte Carlo by taking 2D Fourier transform of the histogram (6a) and by computing the EJCCF Eq. (60) (6b) and from the analytic expressions by Griebsch (6c), Zhylyevskyy (6d), corrected Zhylyevskyy (6e). Zhylyevskyy's plot (6d) is undefined at $(0, 0)$.

ϕ_{G} and ϕ, and the benchmark values are the numerical JCCFs and JCPDFs calculated from Monte Carlo simulations. Please note in order to only show the effects on the discontinuity of the complex plane, we fill the missing value of its JCCF at $(\xi_x = 0, \xi_v = 0)$ with the correct value and then compute the JCPDF. The smaller the RMSE is, the more similar the test values are to the benchmark values. The MAE of two datasets is the maximum absolute difference between each pair of data points, reflecting the variability of the dataset. Here in order to illustrate the variability of the difference of two JCCF expressions regardless of whether they are numerical or analytical, our datasets are the differences between the two sets of values we want to compare. In Table 3, we set the datasets to be the differences between the JCCF or JCPDF

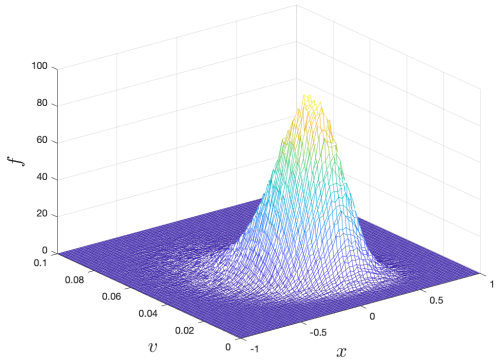

(a) Monte Carlo

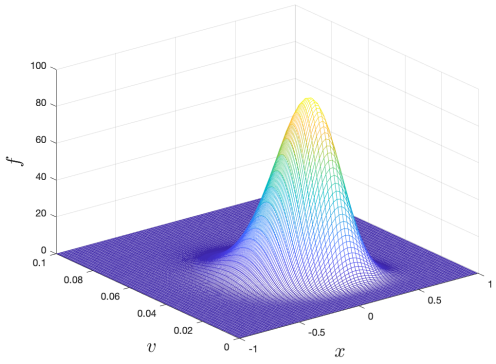

(b) Griebsch

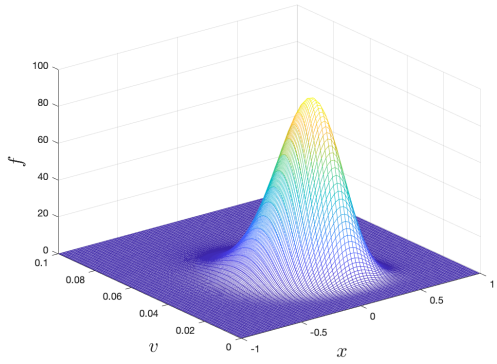

(c) Corrected Zhylyevskyy

Fig. 7: Joint conditional probability density function (JCPDF) at maturity T from a Monte Carlo histogram (7a) and from an inverse 2D Fourier transform of the analytic expressions by Griebsch (7b) and corrected Zhylyevskyy (7c). However as there are undefined value in Zhylyevskyy's JCCF expression, the JCPDF can not be found through Matlab FFT function.

Table 2: Reasonable ranges for randomly generating the Heston model parameters.

	Parameter range
κ	$(0.50, 5.00)$
θ	$(0.01, 0.95)$
σ	$(0.01, 0.95)$
ρ	$(-0.90, 0.10)$
$v(0)$	$(0.01, 0.95)$

calculated from analytical expressions and the corresponding values obtained from MC. We can observe in Table 3, the RMSEs and MAEs obtained from the JCCFs (i.e. ϕ_{Z}, ϕ_{G} and ϕ) and EJCCFs are very small especially for RMSEs of JCCF and EJCCF. This verified the good performance of the Griebsch and the corrected Zhylyevskyy JCCF expressions, which is also shown on the Figs. 6 and 7. When we set the histogram JCCF or histogram approximated JCPDF as benchmark, the corresponding MAEs are still small numbers but relatively higher than they are got when we set JCCF and EJCCF as benchmark. (But the RMSEs for JCPDF is pretty high, explain?) This is because in order to get numerical JCCF from the histogram, we need to apply 2D Fourier transform which contains the numerical error itself. Similarly, we also need to apply 2D inverse Fourier transform on ϕ_{G} and ϕ to get the JCPDF. So the relatively higher error could caused by the numerical error created from the Fourier transform. We can also notice that the RMSEs and MAEs obtained from ϕ are same as those calculated from ϕ_{G}, which verified the two expression are exactly same further regardless the choice of the Heston model parameters. This can be further validate in Table. 4 where we compare them by computing the average the corresponding RMSE and MAE. It is worth mentioning that the high value of MSE in JCPDF is due to the rough surface of the Monte Carlo histogram see Figs. 7a, 7b and 7c. The magnitude of the difference can be visualised in

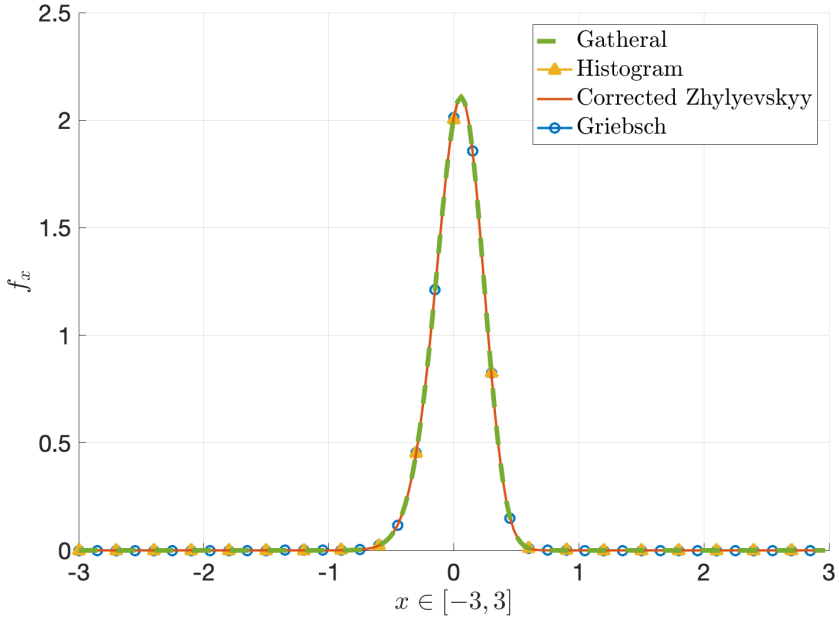

Fig. 8: Marginal conditional probability functions obtained from the histogram, Bakshi ϕ_{H}, corrected Zhylyevskyy ϕ and Griebsch ϕ_{G} with the parameters in Table 1 and the maturity T is 5.

Table 3: Comparison of the analytical JCCF expressions ϕ_{Z} (filled the value at the peak point of ϕ_{Z}), ϕ_{G} and ϕ, and the corresponding JCPDFs with the numerical benchmark results by computing average RMSE and average MAE in 10000 test cases.

	Histogram JCCF		EJCCF		Histogram JCPDF	
	RMSE	MAE	RMSE	MAE	RMSE	MAE
Zhylyevskyy	0.0139	1.5731	0.0040	0.2210	9.5757	5.7881
Griebsch	0.0139	1.5731	0.0040	0.2210	9.5750	5.7872
Corrected Zhylyevskyy	0.0139	1.5731	0.0040	0.2210	9.5750	5.7872

Table 4: Comparison of the Griebsch expression with the other two analytical expressions corrected Zhylyevskyy ϕ and original Zhylyevskyy expressions ϕ_{Z} by computing average RMSE and average MAE in 10000 test cases.

	RMSE	MAE
Corrected Zhylyevskyy ϕ	5.6639×10^{-17}	4.1515×10^{-15}
Original Zhylyevskyy ϕ_{Z}	1.1277×10^{-5}	9.5046×10^{-4}

Fig.9a. The shape of the difference is same as the shape of all JCPDF. So it is reasonable to deduce that the high value of the MSE in JCPDF is due to the roughness of the Monte Carlo histogram not because of the analytical JCCF epression from corrected Zhylyevskyy and Griebsch.

In Table 4, we compare the analytical expressions themselves, by defining the Griebsch JCCF expression ϕ_{G} as the benchmark values and the other two ϕ and ϕ_{Z} as the testing values. We proved in Sect. 2.2, despite $\phi_{\mathrm{Z}}(\xi_x = 0, \xi_v = 0)$ is undefined, the three expressions are analytical equivalent. In order to observe difference caused by the numerical problem i.e. complex discontinuity only in the Zhylyevskyy's JCCF expression, we set the undefined value as $\phi_{\mathrm{Z}}(0,0) = \phi(0,0) = \phi_{\mathrm{G}}(0,0) = 1$ before we compute average RMSE and MAE. As result, we can observe all the RMSEs and MAEs are small, especially for the corrected Zhylyevskyy's average RMSE close to 0, which support our previous proof. However both of the average RMSE and MAE obtained from ϕ_{Z} are relatively higher than those compute from ϕ. This is due to the expression ϕ_{Z} suffers from the numerical discontinuity in the complex plane caused by branch switching which we discussed in Sect. 2.5.

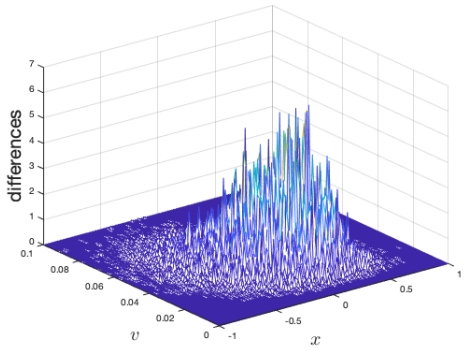

(a) Differences between JCPDF from Monte Carlo histogram and corrected Zhylyevskyy

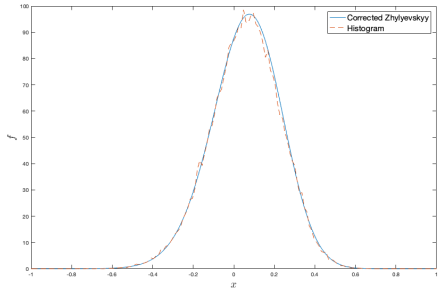

(b) The peak of the difference across the log return

Fig. 9: Left (9a): differences between the JCPDF at maturity T from a Monte Carlo histogram and from an inverse 2D Fourier transform of the corrected analytic expressions by Zhylyevskyy. Right (9b): one slice of 9a which contains the peak of the difference across all log returns.

References

Albrecher H, Mayer P, Schoutens W, Tistaert J (2007) The little Heston trap. Wilmott Magazine pp 83–92, URL https://perswww.kuleuven.be/~u0009713/HestonTrap.pdf

Bakshi G, Cao C, Chen Z (1997) Empirical performance of alternative option pricing models. The Journal of finance 52(5):2003–2049, dOI 10.1111/j.1540-6261.1997.tb02749.x

Broadie M, Kaya Ö (2006) Exact simulation of stochastic volatility and other affine jump diffusion processes. Operations research 54(2):217–231, dOI 10.1287/opre.1050.0247

Cai N, Li C, Shi C (2021) Pricing discretely monitored barrier options: When Malliavin calculus expansions meet Hilbert transforms. Journal of Economic Dynamics and Control 127:104113, dOI j.jedc.2021.104113

Carr P, Madan D (1999) Option valuation using the fast Fourier transform. Journal of Computational Finance 2:61–73, dOI 10.21314/JCF.1999.043

Cui Y, del Baño Rollin S, Germano G (2017) Full and fast calibration of the Heston stochastic volatility model. European Journal of Operational Research 263(2):625–638, DOI 10.1016/j.ejor.2017.05.018

Duffie D, Pan J, Singleton K (2000) Transform analysis and asset pricing for affine jump-diffusions. Econometrica 68(6):1343–1376, dOI 10.1111/1468-0262.00164

Duffie D, Filipović D, Schachermayer W, et al. (2003) Affine processes and applications in finance. The Annals of Applied Probability 13(3):984–1053, dOI 10.1214/aoap/1060202833

Feng L, Linetsky V (2009) Computing exponential moments of the discrete maximum of a Lévy process and lookback options. Finance and Stochastics 13:501–529, dOI 10.1007/s00780-009-0096-x

Fusai G, Abrahams ID, Sgarra C (2006) An exact analytical solution for discrete barrier options. Finance and Stochastics 10:1–26, dOI 10.1007/s00780-005-0170-y

Fusai G, Germano G, Marazzina D (2016) Spitzer identity, Wiener-Hopf factorisation and pricing of discretely monitored exotic options. European Journal of Operational Research 251(1):124–134, dOI 10.1016/j.ejor.2015.11.027

Gatheral J (2011) The volatility surface: a practitioner's guide, vol 357. John Wiley & Sons, dOI 10.1002/9781119202073

Griebsch SA (2013) The evaluation of european compound option prices under stochastic volatility using fourier transform techniques. Review of Derivatives Research 16(2):135–165, dOI 10.1007/s11147-012-9083-z

Heston SL (1993) A closed-form solution for options with stochastic volatility with applications to bond and currency options. Review of Financial Studies 6(2):327–343, dOI 10.1093/rfs/6.2.327

Kahl C, Jäckel P (2005) Not-so-complex logarithms in the Heston model. Wilmott Magazine 19(9):94–103, URL https://bit.ly/3auQDTW

Lord R, Kahl C (2006) Why the rotation count algorithm works. Tinbergen Institute Discussion Paper No. 2006-065/2, dOI 10.2139/ssrn.921335

Lord R, Kahl C (2010) Complex logarithms in Heston-like models. Mathematical Finance: An International Journal of Mathematics, Statistics and Financial Economics 20(4):671–694, dOI 10.1111/j.1467-9965.2010.00416.x

Zhylyevskyy O (2010) A fast Fourier transform technique for pricing American options under stochastic volatility. Review of Derivatives Research 3(1):1–24, dOI 10.1007/s11147-009-9041-6